Comparison of HF radar measurements with Eulerian and Lagrangian surface currents

**Johannes Röhrs · Ann Kristin Sperrevik ·
Kai Håkon Christensen · Göran Broström ·
Øyvind Breivik**

Abstract High-frequency (HF) radar-derived currents are compared with in situ measurements to conclude if the radar observations include effects of surface waves that are of second order in the wave amplitude. Eulerian current measurements from a high-resolution acoustic Doppler current profiler and Lagrangian measurements from surface drifters are used as references. Directional wave spectra are obtained from a combination of pressure sensor data and a wave model. Our analysis shows that the wave-induced Stokes drift is not included in the HF radar-derived currents, that is, HF radars measure the Eulerian current. A disputed nonlinear correction to the phase velocity of surface gravity waves, which may affect HF radar signals, has a magnitude of about half the Stokes drift at the surface. In our case, this contribution by nonlinear dispersion would be smaller than the accuracy of the HF radar currents, hence no conclusion can be made. Finally, the analysis confirms that the HF radar data represent an exponentially weighted vertical average where the decay scale is proportional to the wavelength of the transmitted signal.

Responsible Editor: Matthew Robert Palmer

J. Röhrs (✉) · A. K. Sperrevik · K. H. Christensen · Ø. Breivik
Norwegian Meteorological Institute, Allegaten 70,
5007 Bergen, Norway
e-mail: johannes.rohrs@met.no

G. Broström
Department of Earth Science, University of Gothenburg,
Gothenburg, Sweden

1 Introduction

High-frequency (HF) radars can measure ocean currents by using the radio wave backscatter signal from surface gravity waves (Stewart and Joy 1974). The obtained area-wide current fields have proven useful for assimilation into ocean circulation models (e.g., Zhang et al. 2010, Sperrevik et al. 2015) and as nowcasts in time critical applications like search-and-rescue operations and for oil spill mitigation (Paduan and Washburn 2013; Breivik et al. 2013).

Radio waves emitted by the HF radar are reflected through Bragg backscattering from waves at the ocean surface. The return signal experience a Doppler shift by the apparent phase velocity v_p^{obs} of the scattering waves (Bragg waves), which differs from the intrinsic phase velocity c_p in the presence of an underlying ocean current **v**. The radial component of **v** observed by the radar is

$$v^{(HF)} = c_p^{obs} - c_p. \tag{1}$$

The intrinsic phase velocity c_p is known from the dispersion relation of surface gravity waves and the frequency of the transmitted signal (Stewart and Joy 1974). Applications of HF radars typically employ the dispersion relation for linear waves, but some studies suggest that nonlinear contributions are relevant for HF radar currents (Barrick and Weber 1977; Arduin et al. 2009).

Due to their complex and remote measurement principle, HF radar-derived currents require a more elaborate interpretation than traditional in situ observations (Chapman and Graber 1997). Firstly, the radar receives its information from a horizontal footprint area and a vertical integration rather than measuring at a distinct location. Secondly, the estimated current has been suggested to include the entire, or parts of, the wave-induced Stokes drift (Stokes 1847), but

the literature is inconsistent and sometimes unspecific on what part of the Stokes drift is included. While HF radar currents are usually interpreted as Eulerian currents (i.e., not including the Stokes drift), some studies (e.g., Graber et al. 1997; Law 2001) assume that they include the full Stokes drift. Ardhuin et al. (2009) argue that HF radar currents include only parts of the Stokes drift and compare their measurements with a "filtered Stokes drift" derived by Broche et al. (1983). Ohlmann et al. (2007) compared HF radar currents with drifter observations and underline this problem by remarking that the role of the Stokes drift "may not be reconciled consistently among platforms."

The view that HF radar currents should be Eulerian is motivated by the fact that the radar retrieves its signal from fixed regions in space, hence not following particle motions. The opposing view, that HF radar currents include the Stokes drift, implies that the waves are advected by their own mean drift velocity, which is incompatible with linear theory. Stokes drift contributions to HF radar currents are in fact motivated by a nonlinear correction to the phase velocity (Barrick and Weber 1977) with numeric values similar to the Stokes drift (Broche et al. 1983). Here, we address this problem by comparing HF radar currents to Lagrangian drifter velocities, Eulerian currents from an acoustic Doppler current profiler (ADCP), and wave data that supply the Stokes drift. Since we have ADCP current profiles with high vertical resolution near the surface, our data also allow us to assess what part of the ocean column is observed by the radar.

The main question addressed here is if HF radar measurements represent Eulerian or Lagrangian ocean currents. In the latter case, whether or not the HF radar currents contain a signal from surface waves proportional to the Stokes drift. The theoretical background with regard to the second order wave quantities is briefly presented in Section 2. Our methods and the field data are documented in Section 3. A synthesis between the ADCP, surface drifter, and wave data is presented in Section 4. Section 5 contains a discussion and interpretation of HF radar currents in terms of vertical origin and an assessment of Stokes drift contributions. Our conclusions are summarized in Section 6.

2 Theoretical background

The difference between the Eulerian velocity at fixed position and the Lagrangian (particle following) velocity is, per definition, the Stokes drift. In the presence of surface gravity waves, the Stokes drift arises because particles are for longer time exposed to the forward wave motion while its phase propagates forward (Stokes 1847). The resulting surface net drift in wave propagation direction is at the order of 10 cm s^{-1} for a wind sea with significant wave heights

of 2 m (Röhrs et al. 2012). In deep water, the Stokes drift of surface gravity waves decays exponentially with depth; the decay scale depends on the wave number and is typically of the order 1 m.

2.1 Nonlinear wave effects

Barrick and Weber (1977) derived a second-order correction to the dispersion relation of surface waves using a perturbation technique. This correction is described as resulting from two separate mechanisms: (i) the "self effect," which yields a slightly higher phase velocity of monochromatic waves, and (ii) a "mutual effect" resulting from nonlinear wave-wave interactions. In the latter case, their theory predicts how one wave component influences the phase speed of other components, even in the case when the propagation directions are orthogonal to each other. These second-order effects have later been interpreted in terms of the surface Stokes drift. More specifically, a "filtered Stokes drift" can be obtained by integrating the wave spectrum multiplied by a weighting function that depends on the Bragg wavelength and the direction between the observation point and the HF radar (e.g., Ardhuin et al. 2009).

Creamer et al. (1989) revisited the problem of higher order corrections, and, using Hamiltonian theory, arrived at a result that differs from that of Barrick and Weber. They argue that products of linear and higher order terms largely cancel the second-order corrections obtained by Barrick and Weber. Janssen (2009) later confirmed this result in a more general treatment of the nonlinear problem. Janssen also points out a fundamental problem with the second-order correction terms of Barrick and Weber, namely that important integrated wave parameters such as mean square slope do not converge for high wave numbers.

2.2 Effective depth of HF radar measurements

Stewart and Joy (1974) argue that the vertical origin of the ocean current **v** causing the phase shift in Eq. 1 is related to the wavelength of the scattering Bragg waves. According to their analysis, HF radars observe a vertical average of the ocean current with exponentially decaying weight in radial radar direction as

$$v^{(HF)} = 2k_b \mathbf{e}_\theta \cdot \int_{-\infty}^{0} \mathbf{v}(z)e^{2k_b z} dz, \qquad (2)$$

where z is the depth below surface, k_b is the wave number of the Bragg waves, and $\mathbf{e}_\theta$ the unit vector from the radar towards the observation, with θ being the observation direction of the radar throughout this paper. For typical HF radar transmitter frequencies, the integral in Eq. 2 gives most weight to ocean currents in the upper meter of the ocean.

3 Methods and data

To interpret HF radar currents, we use Lagrangian surface drifters, a Eulerian current meter, and surface wave data. The data was collected during a field experiment in the spring of 2013 on the shelf sea off Vesterålen, Norway (Fig. 1). The main motivation for the HF radar deployment was the assimilation of HF radar currents and hydrography profiles into an ocean model. The research vessel "Johan Hjort," at sea on the annual cod stock assessment cruise of the Institute of Marine Research, was used for deploying surface drifters. Moored current meters were deployed 3 weeks in advance before the vessel arrived in the area.

3.1 Surface drifting buoys

Two types of surface drifters were released from R/V Johan Hjort in the period 16–17 March 2013. Seven iSphere drifters and seven self-locating datum marker buoys (SLDMBs), both manufactured by MetOcean, Canada, were deployed pairwise at the locations shown in Fig. 1. By March 25, all drifters had left the area covered by the radars.

The iSpheres are half-submerged spheres with a diameter of 35 cm without a drogue. A previous experiment (Röhrs et al. 2012) showed that they are driven by the sum of the Eulerian current and the Stokes drift at the surface, with only little wind drag. The effect of the wind drag on this drifter type is up to 50 % of the Stokes drift in magnitude, depending on the local wind and wave conditions. The SLDMBs drifters have a drogue extending from 30 to 120 cm depth

(also referred to as CODE-type drifters). They follow the ocean current at approximately 1-m depth with negligible wind drag (Davis 1985).

Drifter positions were reported every 30 min by the Iridium satellite system. The drifter velocity $\mathbf{v}^{(d)}$ between two positions $\mathbf{x}_i$ and $\mathbf{x}_{i+1}$ is calculated as

$$\mathbf{v}^{(d)} = \frac{1}{2}(\mathbf{x}_{i+2} + \mathbf{x}_{i+1} - \mathbf{x}_i - \mathbf{x}_{i-1}),\qquad(3)$$

which is a weighted average of 30 min average velocity and 90 min average velocity with double weight to the center 30-min period, therefore approximating a noise reduced 1 h average velocity.

3.2 ADCP data

A Nortek Aquadopp ADCP was deployed at the location shown in Fig. 1 (green diamond), collecting data from March 15 to March 31, 2013. The depth of the ADCP below sea level was 8-10 m depending on the tide. The total water depth at this site is 86 m. The relatively high signal frequency of 1 MHz allowed sampling the current in vertical bins of 25 cm.

The instrument was configured in the same way as in a previous experiment (Röhrs et al. 2012), with data being sampled as 2.5 min averages. A Godin-type filter over 60 min in time was applied to achieve similar time filtering as performed by the HF radar. All bins were depth-referenced to the sea surface using the maximum backscatter signal from the surface.

Fig. 1 The experiment site in Vesterålen, Norway. The positions of the three HF radars at Nyksund, Hovden, and Litløy (from north to south) are marked with *red stars*. The location of the ADCP and pressure sensor mooring is marked with a *green diamond*. Trajectories of pairwise deployed iSphere (in *red*) and SLDMB drifters (in *blue*) are drawn as *solid lines*. Typical HF radar coverage (total vectors) is indicated by the *gray arrows*
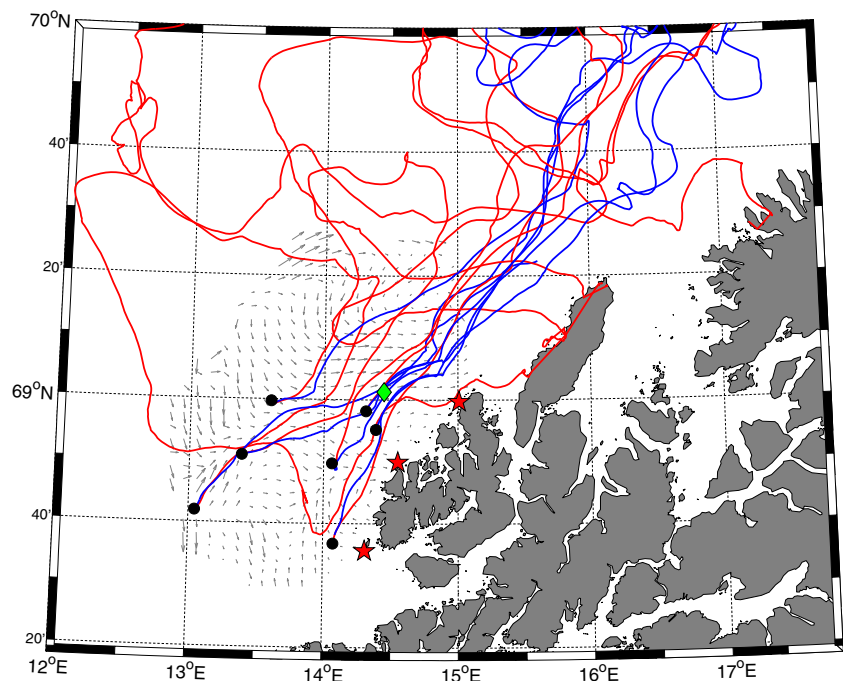
Previous comparisons with surface drifters (Röhrs et al. 2012), as well as comparisons with the surface drifters in this study show that the Aquadopp ADCP, in the configuration used here, provides reliable surface currents at 0.5-m depth: The ADCP current was verified against instantaneous velocities from surface drifters that passed the ADCP mooring within 8 km distance. ADCP currents between 1 and 7-m depth were also verified against a a 600 kHz Aandera ADCP located at 48-m-depth sampling in 1-m bins, which was deployed on the same mooring line. From 0.5 m up to the surface, we assume that the Eulerian (ADCP) currents are constant.

3.3 HF radar currents

Three SeaSonde HF radars manufactured by Codar Ocean Sensors, USA were deployed during March–May 2013 at the locations shown in Fig. 1. The radars used in this experiment are autonomous, rapidly deployable units that were deployed by helicopter. These allow operation in remote areas with no infrastructure (i.e., roads) and mountainous terrain, and are supposed to be deployable in time-critical situations.

The sensors transmitted radio waves of frequency 13.52 MHz and hence measured the Bragg backscatter from surface waves with 11.1 m wavelength and a wave number of $k_b = 0.566$ m^{-1} to retrieve radial current estimates (hereafter called radials). Linear surface waves at this wavelength travel at a phase speed of 4.16 ms^{-1}. Radials were computed using the "MUSIC" algorithm (Schmidt 1986), which provides current estimates in 5° directional bins and 2 km range bins from 3 km to approximately 90 km distance as hourly averages.

As for this experiment, a rapidly deployable HF radar system was used; the radar direction finding algorithm was not calibrated as is common for permanent installations. The origin of each HF radar measurement may therefore exhibit a bearing offset, which was estimated by finding the HF radar directional bin with maximum correlation to radial ADCP currents, as also done by Emery et al. (2004) and Liu et al. (2014). The analysis revealed that the radar at Nyksund has a bearing offset of 5° at the direction towards the ADCP location, while the radar at Hovden has a 30° bearing offset. For the Litløy radar, the ADCP was too far away to assess the bearing direction offset. For this reason, the analysis in this paper focuses on the radials from the Nyksund radar station (northernmost) and disregards the other two radars.

3.4 Wave data

A pressure sensor was used to obtain one-dimensional wave spectra at the experiment site. To obtain the Stokes drift, two-dimensional spectra are needed, and we use a combination of pressure sensor data with results from a numerical model. To evaluate the performance of the model to predict Stokes drift, we use a waverider buoy that is located near the experiment site.

3.4.1 Waves from pressure sensor

Surface wave data at the experiment site were obtained using a TWR-2050 pressure sensor manufactured by RBR, Canada. The instrument was attached to the ADCP mooring. One-dimensional surface wave variance spectra $E(f)$, where f is frequency, are computed from the pressure time series using the standard transfer function. Hourly significant wave heights H_s from the wave spectra are computed according to

$$H_s^{(obs)} = 4\sqrt{\int_0^\infty E(f)df}. \qquad (4)$$

3.4.2 Waves from waverider buoy

A Datawell DWR-MkIII directional waverider buoy moored at 67.56° N, 14.17° E about 160 km south of the experiment site where the total water depth is 220 m. The waverider provided half hourly directional wave spectra $E(f, \theta_w)$, where θ_w is wave direction, in the frequency range of 0.025–0.58 Hz. The Stokes drift at the surface is then computed according to

$$\mathbf{v}_S = 2\int_0^{2\pi}\int_0^\infty E(f, \theta_w)\omega\mathbf{k}df d\theta_w. \qquad (5)$$

Here, $\omega = 2\pi f$ is the wave frequency and $\mathbf{k}$ is the wave number vector.

3.4.3 Waves from numerical weather prediction model

Two-dimensional wave spectra at the experiment site were obtained from the limited area wave model of the European Centre for Medium Range Weather Forecasts (hereafter called LAWAM). This model has about 10 km horizontal resolution and provides hourly directional variance spectra $E(f, \theta_w)$. This wave model has recently been proven useful for predicting Stokes drift profiles (Breivik Ø et al. 2014), which is its main purpose in this study. We compute significant wave height H_s from LAWAM as

$$H_s^{(mod)} = 4\sqrt{\int_0^\infty\int_0^{2\pi} E(f, \theta_w)df d\theta_w}. \qquad (6)$$

The difference between the observed and modeled wave height are used to calculate a correction factor for the model wave energy spectra. A corrected spectra

$$E'(f, \theta_w) = \left(\frac{H_s^{(obs)}}{H_s^{(mod)}} \right)^2 E(f, \theta_w) \tag{7}$$

is used in the analysis, which essentially means that observed wave heights, but modeled propagation directions, are used. The radial component of the Stokes drift in radar observation direction θ is calculated as

$$v_S(z) = \mathbf{e}_\theta \cdot 2 \int_0^{2\pi} \int_0^\infty E' \omega \mathbf{k} e^{2|\mathbf{k}|z} df d\theta_w, \tag{8}$$

To account for unresolved high-frequency contributions, all spectra (including observed spectra) are appended with a f^{-5} spectral tail (Komen et al. 1994).

We also compute an approximation to the nonlinear correction in the phase velocity of Bragg waves, as seen from a HF radar measuring at 0.38 Hz in direction θ_b (Ardhuin et al. 2009):

$$\Delta c_p = \mathbf{e}_\theta \cdot 2 \int_0^{2\pi} \int_0^{0.38Hz} E' \omega \mathbf{k} df d\theta_w$$
$$+ 2k_b \int_0^{2\pi} \int_{0.38Hz}^\infty E' \omega \cos(\theta_w - \theta) df d\theta_w. \tag{9}$$

3.5 Data synthesis

Radials from the HF radar at Nyksund are linearly interpolated to the ADCP position and to the positions of the surface drifters. For comparison with the ADCP, we corrected the bearing direction of the HF radar by 5°, which was found to be the offset of HF radar directions at the ADCP location. The drifter data are averaged over 1 h. A threshold of 2 km separation and a maximum distance of 40 km to the radar station is chosen to find pairs of drifter speed and HF radar currents. In the analysis, we only consider the radial current speed v, that is, the component of the ADCP and drifter velocities along a line from the HF radar towards the observation point. To indicate the contribution of the radial speed to total speed $\mathbf{v}$, we calculate the ratio

$$r_{rad} = \frac{v}{|\mathbf{v}|} \tag{10}$$

for both ADCP currents and drifter velocities, and the ratio

$$r_{S,rad} = \frac{v_S}{|\mathbf{v}_S|} \tag{11}$$

for the Stokes drift radial component compared to total Stokes drift speed $|\mathbf{v}_s|$ given by LAWAM.

The depth-dependent ADCP current $v'^{(A)}(z)$ was vertically integrated from 0 to 7 m depth with an expo-

nentially decaying weight described by a wavenumber k_a:

$$v^{(A)}(k_a) = 2k_a \int_{-z}^0 v'^{(A)}(z) e^{2k_a z} dz. \tag{12}$$

This vertical filter imitates the current measured by the HF radar for $k_b = k_a$, i.e., Eq. 2. To test the hypothesis that HF radar currents include the Stokes drift, we compute the Lagrangian current from the ADCP as

$$v_L^{(A)} = v^{(A)} + v_S. \tag{13}$$

To test the hypothesis that the HF radar currents include a contribution from a nonlinear correction to the phase velocity of Bragg waves Eq. 9, we also compute an Eulerian current with nonlinear correction from ADCP currents:

$$v_{nl}^{(A)} = v^{(A)} + \Delta c_p. \tag{14}$$

Radial components of drifter velocities are denoted as $v^{(d)}$. To obtain Eulerian current estimates from the drifters, we subtract the Stokes drift at the surface for the iSphere drifters and the Stokes drift at 1-m depth for the SLDMB drifters:

$$v_E^{(d)} = v^{(d)} - v_S. \tag{15}$$

Finally, for the drifter data, we compute an Eulerian current with the nonlinear correction term estimated from drifter speeds:

$$v_{E,nl}^{(d)} = v^{(d)} - v_S(z) + \Delta c_p. \tag{16}$$

When comparing HF radar radials with ADCP and drifter speeds, we calculate correlation coefficients r, the slope of linear regression lines S, and the root-mean-square differences (RMS) from the bias-reduced HF radar radials. We also give an estimate on the variation for these three statistics within the presented data: each respective dataset has been re-sampled into 1000 new bootstrapped datasets of the same number of samples (Emery and Thomson 1997, ch. 3.19). Standard deviations were then obtained from the statistics (r, S, and RMS) of the re-sampled data.

4 Results

4.1 Wave data

Significant wave heights from the pressure sensor and from the wave model LAWAM at the ADCP station are shown in Fig. 2a. Observed and modeled wave heights agree well in general, but some discrepancies exist during March 11 to 13 and March 16. To account for these discrepancies, wave spectra used in the analysis are corrected according to Eq. 7 using the observed wave heights from the pressure sensor.

Stokes drift speed and direction from the LAWAM model are shown in Fig. 2b, c along with Stokes drift from the
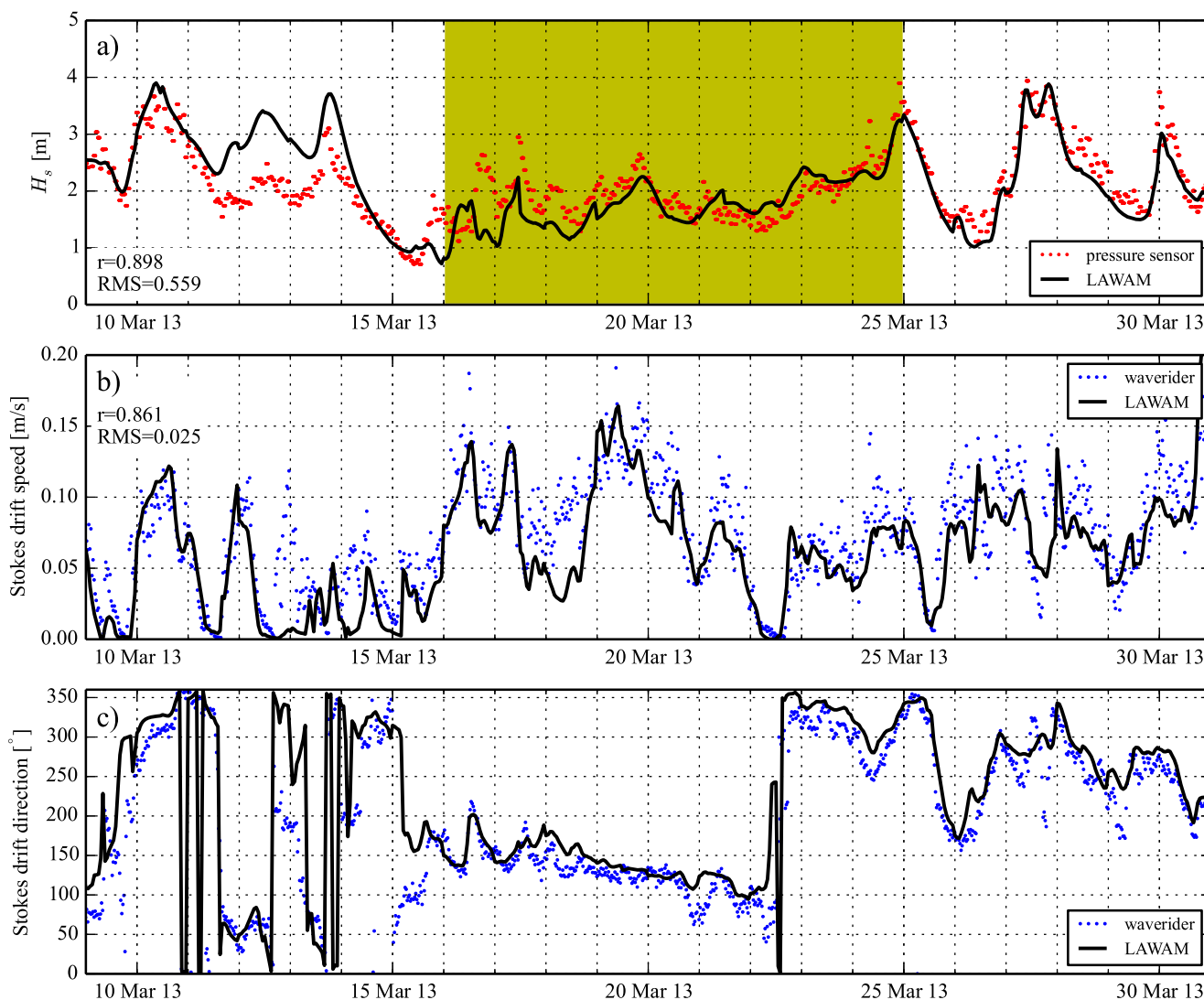
Fig. 2 Comparison of wave model results with observations. **a** Significant wave height from the pressure sensor and from the LAWAM model at the position of the ADCP/pressure sensor rig for the period when ADCP measurements were available. The *yellow shaded area* indicates the period when the drifters are in the range of the HF radar. **b** Stokes drift speed at the surface from the waverider and the LAWAM model at 67.56° N, 14.17° E, which is about 160 km south of the ADCP/pressure sensor rig. **c** Stokes drift direction from the waverider and the LAWAM model for the same position as in panel **b**

waverider. Note that these are not at the same position as the the wave heights in Fig. 2a, but in the same region. To asses the quality of the LAWAM model in our region and time period of interest, correlation coefficients and RMS errors are given for significant wave height and Stokes drift speed in Fig. 2a, b. A vector correlation of Stokes drift components between LAWAM and the waverider is

$$r_v = 1 - \frac{<(v_i - v_j)^2>}{<v_i^2> + <v_j^2>} = 0.903 \qquad (17)$$

where $\mathbf{v}_i$, $\mathbf{v}_j$ are vectors of LAWAM and waverider Stokes drift at the surface, respectively.

Figure 3a shows the Stokes drift at the surface and at one meter depth based on wave spectra from LAWAM, corrected

using Eq. 7, at the position of the ADCP/pressure sensor rig. The Stokes drift at 1 m depth is less than half that of the surface Stokes drift. The figure also shows the nonlinear correction to the phase velocity Δc_p and the Stokes drift at the surface in the waves with frequencies below 0.38 Hz. These are comparable in magnitude to the Stokes drift at 1 m depth. Figure 3c displays the ratio (11) of radial to the total Stokes drift magnitude. Only this fraction can have a possible contribution to the HF radar measurements.

4.2 HF radar compared to ADCP

Comparisons of HF radar radials $v^{(HF)}$ with raw and vertically integrated ADCP speeds are shown in Fig. 4, as

function of depth for the raw ADCP current $v'^A(z)$ and as function of exponential decay scale $z = \frac{1}{2k_a}$ for the integrated $v^{(A)}(k_a)$. For the raw ADCP currents, HF radar currents correlate highest at $z = 1.0$ m depth while the lowest RMS error is at $z = 1.3$ m.

The vertically integrated ADCP current from Eq. 12 agrees best with HF radar currents for decay scales in the range of 0.63 m^{-1} > k_a > 0.36 m^{-1}. This mean that the HF radar signal represents a vertical average of currents weighted by an exponential function with an e-folding scale in the range between 0.8 and 1.4 m. Hence, about 80 % of the HF radar signal comes from the upper meter.

Figure 5 shows scatter plots of HF radar currents versus vertically integrated ADCP currents using $k_a = k_b$ in Eq. 12. The pure Eulerian ADCP current $v^{(A)}$ is shown in panel a, while panel b shows a Lagrangian estimate from ADCP currents $v_L^{(A)}$ that include the Stokes drift calculated by Eq. 8. Panel c shows the comparison for a Eulerian ADCP current $v_{nl}^{(A)}$ that includes the nonlinear correction to the phase velocity of Bragg waves. The Eulerian currents (panels a and c) provide a better fit than the Lagrangian current (panel b). In terms of linear regression slope S and spread (RMS), the pure Eulerian current $v^{(A)}$ shows clearly the best agreement with the HF radar. $v^{(A)}$ also yields the highest correlation coefficient with the HF radar, but this difference does not exceed the uncertainty margins. The scatter plots indicate the fraction of the radial ADCP current relative to the absolute ADCP current in color shading, and it appears that outliers are not related to this ratio, implying that the quality of the radial HF radar current does not depend on the orientation of the total current vector.

4.3 HF radar compared to drifters

A comparison between HF radar radials and drifter speeds is given in Fig. 6. Panel a shows a scatter plot for the Lagrangian current $v^{(d)}$, panel b the Eulerian current estimate $v_E^{(d)}$, and panel c shows an Eulerian estimate with nonlinear correction term $v_{E,nl}^{(d)}$. In contrast to the comparison with the ADCP, the in situ measurements now provides Lagrangian velocities and the subtraction of the Stokes drift gives an Eulerian estimate. The Eulerian current $v_E^{(d)}$ compares better with the HF radar than the Lagrangian current $v^{(d)}$, judging from the difference in linear regression slope S and spread (RMS) relative to their uncertainty margins.

The Eulerian current estimate with nonlinear correction $v_{E,nl}^{(d)}$ performs better than $v_E^{(d)}$ in terms of correlation coefficient r and worse in terms of linear regression slope S and spread (RMS). These differences between the Eulerian current with and without nonlinear correction, however, lie within the uncertainty margins for the drifter vs. HF radar comparison.

The outliers in Fig. 6, noticeable by drifter velocities above 0.7 ms^{-1}, are associated with large distances of 30–40 km between the respective drifter and the HF radar. These outliers cause large RMS values, but are not removed from the analysis because not all samples within this distance range are outliers, indicating that the HF radar was often capable of accurately measuring currents up to 40 km away from the radar.

5 Discussion

5.1 Discrepancies between HF radar currents and in situ observations

While the in situ measurements provide currents at certain points or along trajectories, the HF radar provides spatial and temporal averages. Because the instruments measure different currents, we might expect discrepancies that exceed the error margins and noise of the respective instruments. Expected differences between ADCP and HF radar measurements on the West Florida shelf were recently estimated by Liu et al. (2014), finding that 80–100 % of the observed differences could be explained by the horizontal and vertical separation between the measurements.

While it is possible to eliminate the sampling difference due to temporal averaging (it is straightforward to perform time filtering of ADCP or drifter data), the spatial averaging cannot be synchronized. The HF radar processing algorithm estimates the source of each retrieved backscatter signal and averages all data originating from cells of the same radial range and sector bins. Furthermore, the radar provides the standard deviation for the averaged velocity estimate of each cell. For the radar station at Nyksund, the mean of the spatial standard deviations of all cells is $\sigma_s = 0.095$ ms^{-1}. This is the spatial variability that is typically lost by averaging over the data in each cell. For each cell, a resulting spatial standard error can be estimated (Everitt B 2003) as

$$e_s = \frac{\sigma_s}{\sqrt{N}}, \tag{18}$$

where N is the number of samples for each respective cell. On average, the HF radar at Nyksund provided $\overline{N} = 3.2$ spatially varying samples, ranging from 1 to 26. A temporal standard error e_t can be estimated in a similar way. Values of spatial and temporal standard errors, averaged over all cells, are given in Table 1.

In addition to the differences in averaging, HF radar and in situ currents differ by the extent to which the Stokes drift may be included, and by the depth that is
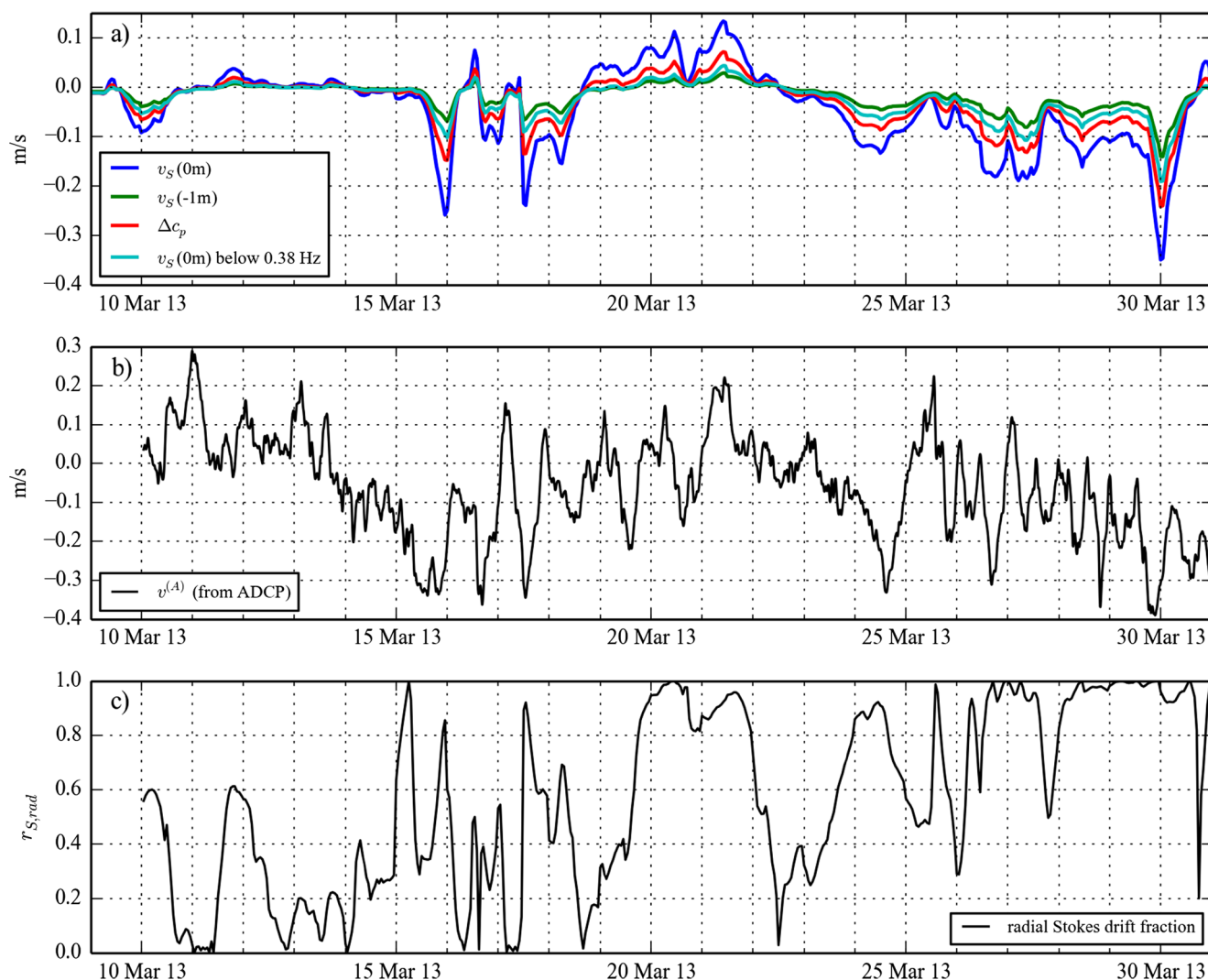
Fig. 3 a Stokes drift at the surface (*blue*) and at one meter depth (*green*) calculated from LAWAM wave spectra at the position of the ADCP station. Also shown is the Stokes drift at the surface for wave frequencies below 0.38Hz (*cyan*) and the nonlinear correction to the phase velocity of Bragg waves Δc_p (*red*). **b** The

Eulerian current measured by the ADCP. All quantities are radial components, pointing from the Nyksund HF radar station towards the ADCP station. **c** Fraction of the Stokes drift component in radial HF radar direction compared to total Stokes drift speed at the surface

sampled by the different instruments. Despite the differences in spatial averaging and instrument noise, we expect that comparisons between the HF radar and the ADCP or drifters yield a higher degree of agreement if the differences in sampling depth and Stokes drift contribution are correctly accounted for, which is the main question in this analysis.

5.2 Vertical origin of HF radar currents

The ADCP data (Fig. 4) with 25 cm vertical resolution and coverage up to 0.5 m below the surface shows that more than 80 % of the HF radar signal originates from the upper meter. The wave number of the Bragg waves ($k_b = 0.566$ m^{-1}) is within the range of the decay scale estimated from

comparison between ADCP and HF radar. Best agreement between HF radar and ADCP was obtained when the ADCP current was vertically integrated according to Eq. 12 with $k_a = k_b$. The theoretical arguments of Stewart and Joy (1974) are thereby confirmed, that is, the radar backscatter signal is exposed to a Doppler shift by the Eulerian current with the same vertical origin as the Stokes drift profile of the Bragg wave.

Teague et al. (2001) compared HF radar currents with ADCP data that was resolved up to 2 m below the surface, employing radars signals with different frequencies. They suggested that the HF radar samples the current at the depth $z = (2k_b)^{-1}$, but did not compare the HF radar currents with vertically integrated ADCP currents. Their ADCP data resolved a depth with minimal RMS error at

Fig. 4 Correlation and RMS deviation between HF radar and ADCP current as function of depth of ADCP current. The *dashed line* shows statistics for ADCP currents at fixed depth. The *solid line* shows statistics for vertically integrated ADCP current, with integration according to Eq. 2 with $k_a = (2d)^{-1}$. The *gray solid line* indicates the depth $(2k_b)^{-1} = 0.88$ m according to the wave number of the used Bragg waves
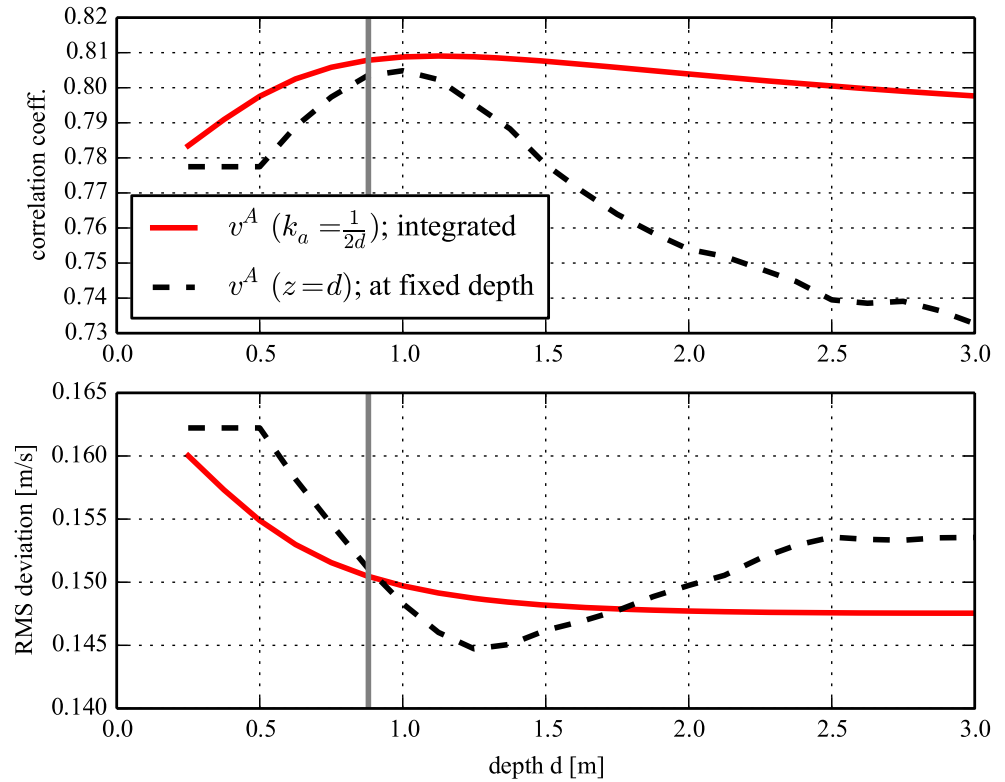
4 m depth for a low frequency radar operating at 4.8 MHz. For a radar frequency of 13.52 MHz, we observe a minimal RMS error at 1.25 m when using ADCP data at fixed depth.

More precisely, the HF radar does not measure the current at $z = (2k_b)^{-1}$ but observes vertically integrated currents, which also gives best agreement between ADCP and the HF radar data presented here. For practical use, however, the vertical origin of HF radar currents is often referred to as an effective depth. Our data supports the practice to use a depth of $z = 0.8$–1.4 m for radars transmitting at 13.52 MHz.

5.3 Contribution of Stokes drift to HF radar currents

By comparing HF radar currents with in situ measurements of Eulerian and Lagrangian currents, we find that (i) the speeds observed by the ADCP agree better with the HF radar if the Stokes drift is not added to the Eulerian ADCP current, and (ii) the current speeds inferred from drifter trajectories agree better with the HF radar currents if the Stokes drift is subtracted from the (Lagrangian) drifter velocity.

Both comparisons lead to the same conclusion that the HF radar measures the Eulerian and not the Lagrangian current. We know from previous experiments that the iSphere

Fig. 5 Scatter plot comparing HF radar currents with ADCP currents. **a** shows the Eulerian ADCP current $v^{(A)}$, **b** shows the Lagrangian current estimate $v_L^{(A)}$ obtained from ADCP and the Stokes drift, and **c** shows the Eulerian current $v_{nl}^{(A)}$ with the nonlinear correction term. The colors of each dot indicate the fraction r_{rad} of radial speed to ADCP total speed (10), with *dark red* for $r_{rad} = 1$ and *bright yellow* for $r_{rad} = 0$
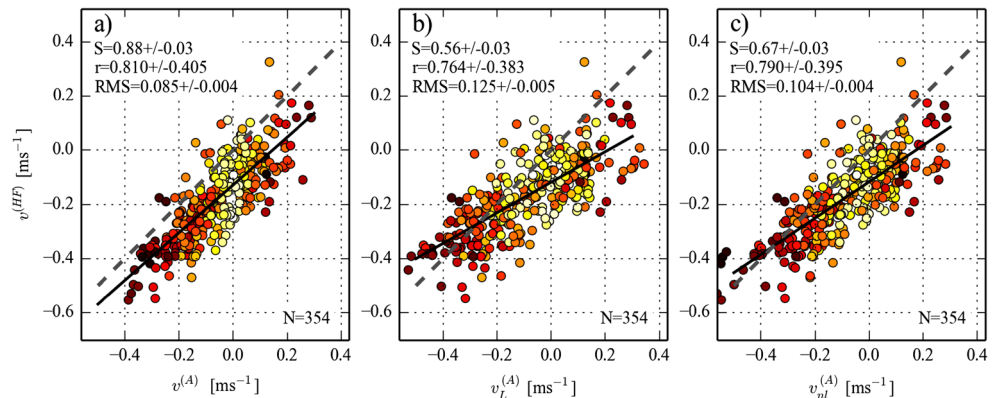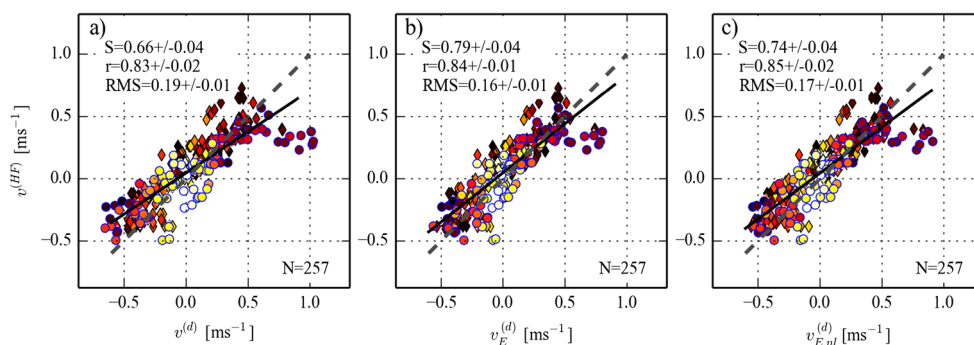
Fig. 6 Scatter plot comparing HF radar currents with drifter speed. *Circles with black edge color* represent iSphere drifters and *diamonds with blue edge color* represent SLDMB speed. **a** Shows the Lagrangian drifter speed v^d, **b** shows the Eulerian current $v_E^{(d)}$ obtained by subtracting the Stokes drift at the respective drifter depth from the drifter speed, and **c** shows the Eulerian current with nonlinear correction term $v_{E,nl}^{(d)}$. The colors of each dot indicate the fraction r_{rad} of radial speed to total drifter speed (10), with *dark red* for $r_{rad} = 1$ and *bright yellow* for $r_{rad} = 0$

Table 1 Magnitudes of the components that form the signal observed by a HF radar transmitting at 13.52 MHz

Phase velocity c_p of linear surface waves	4.16 ms^{-1}
Radial HF radar current $v^{(HF)}$	0.16 ± 1.5 ms^{-1}
Onlinear correction Δc_p	0.03 ± 0.06 ms^{-1}
Spatial error e_s	0.052 ms^{-1}
Temporal error e_t	0.049 ms^{-1}

The values for HF radar current and nonlinear correction averages are derived from the data presented in this study and generally depend on the local current and wave climatology

drifters sample the Lagrangian current, which includes the surface Stokes drift (Röhrs et al. 2012). If the HF radar current is Eulerian, the difference $v^{(HF)} - v^{(d)}$ for the iSphere drifters will be correlated with the Stokes drift. In Fig. 7a, we show the results of such a test: the correlation ($r = -0.721$) is significant within the 99 % level. Figure 7b shows the difference $v^{(HF)} - v^{(d)}$ for the SLDMB drifters, which appears to be independent of Stokes drift. A reasonable explanation is that the SLDMB drifters are following the currents at 1 m depth where the Stokes drift is rather small compared to the surface (compare Fig. 3). Figure 7

also shows (color coded) the ratio $r_{S,rad}$ of the radial Stokes drift component compared to total Stokes drift, as defined in Eq. 11. For the iSphere drifter, there is a clear association of high $r_{S,rad}$ with large deviation between drifter speed and HF radar speed, confirming that the Stokes drift can explain the difference.

A similar comparison for the ADCP current ($v^{(HF)} - v^{(A)}$) is not correlated with the Stokes drift ($r = 0.021$), confirming that both the HF radar and the ADCP measure the Eulerian current. To reason why the HF radar currents do not include the Stokes drift, we recall its measurement

Fig. 7 Comparison between the Stokes drift and the residual current given by the difference between HF current and drifter current for (**a**) the iSphere drifters at the surface and (**b**) the SLDMB drifters at 1 m depth. The radial Stokes drift component for the respective drifter position is color coded with dark red for $r_{S,rad} = 1$ and white for $r_{S,rad} = 0$
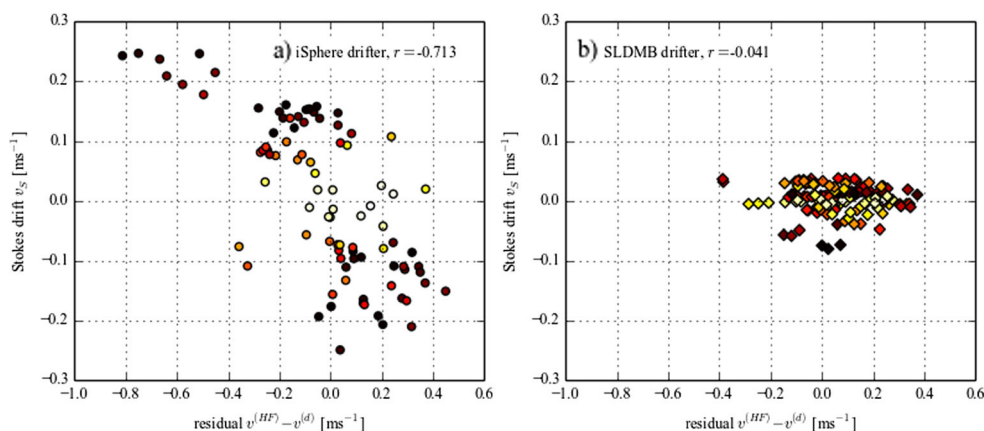
principle: The radar observes the phase speed of surface gravity waves, which is modified by the Doppler shift due to an Eulerian current. The Stokes drift is not a part of the Eulerian current that causes the Doppler shift, and neither should it significantly modify the intrinsic phase velocity of the Bragg waves.

A contribution from nonlinear dispersion (9) appears to be about half of the Stokes drift in magnitude (see Fig. 3). It contains the Stokes drift of waves longer than the Bragg waves (Fig. 3, cyan line) and an additional contribution from shorter waves. A comparison of HF radar currents with Eulerian current estimates with and without the nonlinear correction term (9) from ADCP and surface drifters (Figs. 5 and 6) shows that pure Eulerian estimates yield better agreement. However, the difference is small because the nonlinear correction term itself is small.

Recalling typical magnitudes of the quantities that form the signal measured by the HF radar (Table 1), we conclude that the contribution from the nonlinear phase velocity correction term is smaller than the observation uncertainties of the HF radar currents. This correction term was presented through a series of papers (Broche et al. 1983; Ardhuin et al. 2009) that are based on the analysis of Barrick and Weber (1977), which Creamer et al. (1989) and Janssen (2009) have argued is incorrect, as outlined in Section 2.1. The uncertainty margins of the comparison statistics do not allow for a conclusion on the contribution of this second-order quantity.

6 Conclusions

The presented data allow us to conclude that the HF radar essentially measures the Eulerian current and not the Lagrangian current that includes the Stokes drift. The possible contribution from a nonlinear correction to the phase velocity of the Bragg waves is not significant compared to the uncertainties in the current estimates. The SLDMB drifters in the design of Davis (1985), which follow the current at 1 m depth, are found to be the most suitable in situ platforms for validating HF radar currents because they represent a similar vertical average of ocean currents, and the advection by the Stokes drift for this kind of drifters is small for the wind and wave conditions typical of the area considered in this study.

References

Ardhuin F, Marie L, Rascle N, Forget P, Roland A (2009) Observation and estimation of lagrangian, stokes, and eulerian currents induced by wind and waves at the sea surface. J Phys Oceanogr 39(11):2820–2838. doi:10.1175/2009JPO4169.1

Barrick DE, Weber BL (1977) On the nonlinear theory for gravity waves on the ocean's surface. part ii: Interpretation and applications. J Phys Oceanogr 7(1):11–21

Breivik O, Allen A, Maisondieu C, Olagnon M (2013) Advances in Search and Rescue at Sea. Ocean Dynam 63:83–88. doi:10.1007/s10236-012-0581-1

Breivik Ø, Janssen PEAM, Bidlot JR (2014) Approximate stokes drift profiles in deep water. J Phys Oceanogr 44:2433–2445. doi:10.1175/JPO-D-14-0020.1

Broche P, de Maistre JC, Forget P (1983) Mesure par radar dcamtrique cohrent des courants superficiels engendrs par le vent. Oceanol Acta 6:43–53

Chapman RD, Graber HC (1997) Validation of hf radar measurements. Oceanography 10:76–79. doi:10.5670/oceanog.1997.28

Creamer DB, Henyey F, J Wright RS (1989) Improved linear representation of ocean surface waves. J Fluid Mech 205:135–161. doi:10.1017/S0022112089001977

Davis RE (1985) Drifter observations of coastal surface currents during CODE: The method and descriptive view. J Geophys Res 90(C3):4741–4755. doi:10.1029/JC090iC03p04741

Emery BM, Washburn L, Harlan JA (2004) Evaluating radial current measurements from codar high-frequency radars with moored current meters. J Atmos Ocean Tech 21(8):1259–1271

Emery W, Thomson RE (1997) Data Analysis Methods in Physical Oceanography. Elsevier, Amsterdam

Everitt B (2003) The Cambridge Dictionary of Statistics. Cambridge Univ Press

Graber HC, Haus BK, Chapman RD, Shay LK (1997) HF radar comparisons with moored estimates of current speed and direction: Expected differences and implications. J Geophys Res 102 C8:18 766:749–18. doi:10.1029/97JC01190

Janssen P (2009) On some consequences of the canonical transformation in the Hamiltonian theory of water waves. J Fluid Mech 637(1):1–44. doi:10.1017/S0022112009008131

Komen GJ, Cavaleri L, Doneland M, Hasselmann K, Hasselmann S, Janssen PAE (1994) Dynamics and modelling of ocean waves

Law K (2001) Measurements of near surface ocean currents using hf radar. PhD thesis, University of California Santa Cruz

Liu Y, Weisberg RH, Merz CR (2014) Assessment of codar seasonde and wera hf radars in mapping surface currents on the west florida shelf. J Atmos Ocean Tech 31:1363–1382. doi:10.1175/JTECH-D-13-00107.1

Ohlmann C, White P, Washburn L, Terrill E, Emery B, Otero M (2007) Interpretation of coastal hf radar-derived surface currents with high-resolution drifter data. J Atmos Ocean Tech 24:666–680. doi:10.1175/JTECH1998.1

Paduan JD, Washburn L (2013) High-frequency radar observations of ocean surface currents. Annu RevMarine Sci 5:115–136. doi:10.1146/annurev-marine-121211-172315

Röhrs J, Christensen KH, Hole LR, Broström G, Drivdal M, Sundby S (2012) Observation-based evaluation of surface wave effects on currents and trajectory forecasts. Ocean Dynam 62:1519–1533. doi:10.1007/s10236-012-0576-y

Schmidt (1986) Multiple emitter location and signal parameter estimation. IEEE T Antenn Propag 34-3:276–280. doi:10.1109/TAP.1986.1143830

Sperrevik AK, Christensen KH, Röhrs J (2015) Constraining energetic slope currents through assimilation of high-frequency radar observations. Ocean Sci 11:237–249. doi:10.5194/os-11-237-2015

Stewart RH, Joy JW (1974) HF radio measurements of surface currents. Deep Sea Res 21:1039–1049. doi:10.1016/0011-7471(74)90066-7

Stokes GG (1847) On the theory of oscillatory waves. Trans Cambridge Philos Soc 8:441–473

Teague C, Vesecky J, Hallock Z (2001) A comparison of multifrequency hf radar and adcp measurements of near-surface currents during cope-3. IEEE J Ocean Eng 26(3):399–405. doi:10.1109/48.946513

Zhang WG, Wilkin JL, Arango HG (2010) Towards an integrated observation and modeling system in the New York Bight using variational methods. Part I: 4DVAR data assimilation. Ocean Model 35:119–133. doi:10.1016/j.ocemod.2010.08.003